ADAPTIVE OPTICS IMAGING OF PARAFOVEAL CONES IN TYPE 1 DIABETES

MARCO LOMBARDO, MD, PHD,* MARIACRISTINA PARRAVANO, MD,* GIUSEPPE LOMBARDO, MENG, PHD,†‡ MONICA VARANO, MD,* BARBARA BOCCASSINI, MD,* MARIO STIRPE, MD,* SEBASTIANO SERRAO, MD, PHD*

Purpose: To evaluate the parafoveal cone density in patients with Type 1 diabetes mellitus (DM1).

Methods: Adaptive optics retinal images of the photoreceptor mosaic were acquired from 11 DM1 patients (study group) and 11 age-matched healthy subjects (control group). Cone density was analyzed, along the horizontal and vertical meridian, at 230-μm, 350-μm, and 460-μm eccentricity from the fovea. Central retinal thickness was measured using a Spectralis spectral-domain optical coherence tomography. A multiple regression model was performed to determine the relationships between the explanatory variables (age, glycohemoglobin level, presence of diabetic retinopathy, duration of diabetes, and central retinal thickness) and cone density.

Results: Patients had a diagnosis of DM1 in the past 9 years to 21 years. Of these, five patients had a diagnosis of no diabetic retinopathy and six had mild nonproliferative diabetic retinopathy. On average, cone density was 10% lower in the study than in the control group at each retinal eccentricity along the horizontal and vertical meridians (analysis of variance, $P < 0.001$). The central retinal thickness was thicker in DM1 eyes than in the control eyes (278 ± 20 μm and 260 ± 13 μm; $P < 0.05$). The model explained 61% ($P < 0.01$) of the variance of cone density in the population, with the variables representing an abnormal glucose metabolism, that is, a higher glycohemoglobin level, the presence of diabetic retinopathy, and a chronic diabetes, having the highest influence on cone density decline.

Conclusion: A subtle decrease of parafoveal cone density was found in DM1 patients in comparison with age-matched control subjects via high-resolution adaptive optics retinal imaging. The cone density decline was moderately associated with a disturbance in the glucose metabolism.

RETINA 0:1–12, 2013

Diabetic retinopathy (DR) is a serious and frequently occurring complication of diabetes mellitus. It represents the leading cause of new cases of blindness among adults in the Western world: the estimated proportion of blindness as a result of DR is 15% to 17% in the Americas and Europe.[1–3] It can be classified as nonproliferative (NPDR) or proliferative. Nonproliferative diabetic retinopathy is further graded in mild, moderate, and severe according to the Early Treatment Diabetic Retinopathy Study severity scale.[4] According to the most commonly accepted pathophysiologic model (microvascular theory),[5–7] DR consists of a microangiopathy that induces pathologic changes of the vascular structures and in the blood rheological properties as a consequence of chronic hyperglycemia. All these factors contribute to increased capillary permeability and capillary occlusion, and accordingly to retinal ischemia, leading to the major complications of DR, which include the generation of new retinal–vitreal vessels and retinal detachment. Diabetic retinopathy has

From the *Fondazione G.B. Bietti IRCCS, Rome, Italy; †CNR-IPCF Unit of Support Cosenza, University of Calabria, Rende, Italy; and ‡Vision Engineering, Rome, Italy.

Supplemental digital content is available for this article. Direct URL citations appear in the printed text and are provided in the HTML and PDF versions of this article on the journal's Web site (www.retinajournal.com).

None of the authors have any financial/conflicting interests to disclose.

Reprint requests: Marco Lombardo, MD, PhD, Fondazione G.B. Bietti IRCCS, Via Livenza 3, Rome 00198; e-mail: mlombardo@visioeng.it

Copyright © by Ophthalmic Communications Society, Inc. Unauthorized reproduction of this article is prohibited.

been also theorized as a multifactorial disease involving the retinal neuronal cells (neurodegenerative theory).[8–10] The neurodegenerative changes are apoptosis of several populations of retinal cells, including photoreceptors, bipolar cells, ganglion cells, and astrocytes. Structural and functional impairments of the neural tissue are supposed to contribute to the earliest alterations of the vascular structures.[8–12]

Experimental evidence of apoptotic death of cone photoreceptors and necrotic degeneration of neuronal cells has been provided in drug-induced diabetes.[13] In addition to microangiopathy, nonnecrotic photoreceptor loss has been therefore theorized to be responsible for the pathologic alteration of cones associated with diabetes.[14,15] As far as we know, there has been no attempt to investigate whether cone loss may occur in patients with diabetes during the early DR stage.

Noninvasive clinical detection of DR is usually performed by dilated fundus examination, color fundus photography, and more sophisticated retinal imaging techniques, including scanning laser ophthalmoscopy and spectral-domain optical coherence tomography (SD-OCT). Adaptive optics (AO) technology[16] permits to obtain high-resolution images of the retina, which allows the visualization of photoreceptors, capillaries, and nerve fiber bundles. In the present study, we aimed to evaluate the parafoveal cone density in a series of patients diagnosed with Type 1 diabetes mellitus (DM1) within the past 9 years to 21 years and no or mild signs of DR and to correlate it with the duration of diabetes, the glycohemoglobin serum level, the presence of DR, and the SD-OCT retinal thickness measurement.

Materials and Methods

Patients diagnosed with DM1 participated in this study and signed an informed consent after full explanation of the procedure. Inclusion criteria were older than 18 years, diagnosis of DM1 from at least 1 year beforehand, no or mild signs of NPDR according to the Early Treatment Diabetic Retinopathy Study severity scale,[4,17] and 20/20 or better best-corrected visual acuity. Exclusion criteria were astigmatism higher than 3.00 diopters, the presence of any ocular disease, including ocular media opacities, or previous eye surgery. Age-matched voluntary healthy subjects were included in the study as control subjects. Control subjects had no history of systemic or ocular diseases and no previous eye surgery.

The study protocol had the approval of the local ethical committee and adhered to the tenets of the Declaration of Helsinki. All subjects received a complete eye examination, including a noncontact ocular biometry using the IOL Master (Carl Zeiss Meditec AG, Hennigsdorf, Germany), retinal imaging using Spectralis SD-OCT (Heidelberg Engineering GmbH, Heidelberg, Germany), a digital ophthalmoscope (F10; Nidek Co, Ltd, Tokyo, Japan), and color fundus photography (TRC-50 DX; Topcon Instrument, Corp, Tokyo, Japan). An MP1 microperimetry (Nidek Co, Ltd) was performed to determine the central 10° retinal sensitivity: a grid of 37 stimuli, with Goldmann III stimulus size, 200-millisecond duration, and a 4-2 threshold strategy was used. Numeric thresholds (in decibels) were exported for statistical analysis.

Adaptive Optics Retinal Imaging and Image Analysis

An AO retinal camera prototype (rtx1; Imagine Eyes, Orsay, France) was used to image the cone mosaic.[18,19] Adaptive optics imaging sessions were conducted after dilating the pupils with 1 drop of 1% tropicamide. Both eyes of each subject were imaged. During AO imaging, each patient was instructed to fixate the internal target of the instrument moved by the investigator at specific retinal locations, considering that the fixation coordinates ($x = 0°$ and $y = 0°$) correspond to the foveal fixation reference point. A video camera monitored the subject's pupil and eye movements. Digital videos were recorded on 16 locations surrounding fixation, extending 4° nasal and temporal and 1.8° superior and inferior from fixation. Additional videos were recorded in regions of interest. For each location, a video of 40 frames (4° field size) was captured by the retinal camera. After acquisition, a proprietary program provided by the manufacturer has been used to correct for distortions within the frames of the raw image sequence and to correlate and frame-average to produce a final image with enhanced signal-to-noise ratio before further analysis. Frames exhibiting large motion artifacts because of eye movement or blinking (on average <5 frames per acquisition) were manually removed before processing.

The image cone labeling process was performed using an algorithm implemented with the image processing toolbox in Matlab (Mathworks, Inc, Natick, MA), as previously described by Li and Roorda[20] with some enhancements. Filtering and morphologic image processing were applied to isolate the higher intensity signals corresponding to, presumably, cone photoreceptors. Filtering parameters were manually selected based on the estimated minimum diameter of two adjacent cones to avoid potential mistakes by eliminating locations that were too close together to the cones. The value of the filtering parameter[20] varied between 10 pixels and 15 pixels according to the eccentricity location where cones were labeled. An empirically determined intensity threshold (0.18 peak intensity of the image normalized

Copyright © by Ophthalmic Communications Society, Inc. Unauthorized reproduction of this article is prohibited.

to 1) was applied on the set of identified local maxima to further reduce false-positives. Cone density measures were performed by an independent expert observer (G.L.) who was not informed about the group membership of the images. Manual editing was performed by the same user to identify the cones missed or misinterpreted by the automated algorithm. During manual editing, the brightness and contrast of each image was adjusted by the observer to assist in determining whether a cone was present. This procedure was previously shown to significantly reduce the error of interobserver variability.[21]

For each location, cone density was calculated after manual checking in all cases. Cone density (cones/square millimeter) was estimated, within two 50 μm × 50 μm sampling windows, at specific eccentricities from the fovea (±230 μm, ±350 μm, and ±460 μm) along the horizontal and vertical meridians. Eccentricity was computed as the distance between the center of each sampling window and the foveal fixation reference point ($x = 0°$ and $y = 0°$).

The *x-y* coordinates of the labeled cones were stored, and the center-to-center cone distances ("inter-cone distance [ICD]" or "cone spacing," in micrometers) were calculated from them under the assumption that they were hexagonally arranged.[21,22] Under this assumption, the cone spacing is determined from density counts by the following: $\mathrm{ICD} = 1,000[\frac{2}{\sqrt{3D}}]^{1/2}$, where D is the number of cones per square millimeter.

The sampling window size, cone density and spacing, and eccentricity data were corrected based on axial length and refractive error of the individual eye according to the nonlinear formula of Drasdo and Fowler[23] and using the Gullstrand eye as a model, as previously shown.[18,19,23–25] The spectacle-corrected magnification factor ($\mathrm{RMF_{corr}}$) was calculated to correct for the differences in optical magnification and thus retinal image size between the eyes. The $\mathrm{RMF_{corr}}$ was estimated for each eye by consideration of the axial length and the trial lens added to the system to compensate for defocus. The spectacle vertex distance was set at 14 mm for all eyes.

In each eye, the final AO images were further automatically stitched together to create a larger montage image of the photoreceptor mosaic using a commercial software (Photomerge tool, Photoshop Version CS3; Adobe, San Jose, CA). This procedure was used, for reference purposes, to compare the AO images with the wide-field scanning laser ophthalmoscopy image and color fundus photographs.[18]

Spectral-Domain Optical Coherence Tomography Image Analysis

Spectral-domain optical coherence tomography images were acquired in each eye using a volume scan 10° × 15° in the high-resolution modality (numbers of B-scans, 13; distance between each scan, 240 μm; real-time averaging algorithm, 50 frames). The Spectralis software automatically provided two contour lines that were positioned at the layers of interest for segmented measurements of the retinal thickness. In this study, central retinal thickness (CRT), central outer nuclear layer thickness (ONL), and central photoreceptor layer (PL) thickness were manually measured along the horizontal (nasal, temporal) scan and the vertical (inferior, superior) scan passing through the fovea: measurements were obtained at the fovea and at 230 μm, 350 μm, and 460 μm away from the fovea. The CRT, ONL, and PL were calculated by taking the average of the horizontal and vertical measurements. The CRT was defined as the distance between the internal limiting membrane and the outer edge of the retinal pigment epithelium; the ONL was defined as the distance between the posterior boundary of outer plexiform layer and the external limiting membrane; the PL was defined as the distance between the external limiting membrane and the inner edge of the retinal pigment epithelium. The inner retinal complex was accordingly defined as the difference between the CRT and both the ONL and PL thicknesses.

Spectral-domain optical coherence tomography thickness measurements were taken by two independent observers who were masked to the patient group. All SD-OCT images were corrected according to the biometric data of each eye. Automated retinal thickness measurements of the 1-mm central Early Treatment Diabetic Retinopathy Study area, as provided by the Spectralis software, were recorded in each subject for comparison with the manually registered CRT.

Statistical Analysis

The repeatability of cone density measurements, performed on two 50 μm × 50 μm sampling windows at the same eccentricity location by the automated algorithm, was calculated based on the within-subject standard deviation (σ_w), that is, the common standard deviation of repeated measurements. To get the common σ_w, we averaged the variances, that is, the squares of the standard deviations of the two repeated measures for each subject. The σ_w was chosen as an index of measurement error, as discussed by Bland and Altman.[26,27] The repeatability was defined as $2.77\sigma_w$ and reported both in terms of the measurement unit and as a percentage of the mean. The 95% confidence interval for repeatability was calculated as $\frac{2.77\sigma_w}{\sqrt{2n(m-1)}}$, where n is the number of subjects and m is the number of observations for each subject.

Cone metrics and SD-OCT values, estimated at equivalent retinal eccentricity locations of fellow eyes,

Copyright © by Ophthalmic Communications Society, Inc. Unauthorized reproduction of this article is prohibited.

were averaged in each subject and used for analysis. The repeated-measures analysis of variance was performed for the statistical analysis of cone density at each eccentricity along the horizontal and vertical meridians. The coefficient of variation was used to analyze the variation of cone density across subjects of the same group. A multiple regression analysis (linear mixed model) determined the relationships between the explanatory variables (age, duration of diabetes, glycohemoglobin serum level, diabetes status—defined as the absence or presence of DR—and CRT) and cone density. A principal component analysis was performed to determine the weighted influence of the above variables on cone density estimates and whether those variables contributed in the same way (i.e., they were correlated) or independently from each other.

Statistical significance was set at $P < 0.05$ for all the tests performed.

Results

Eleven DM1 patients (5 men and 6 women; age range, 33–51 years; mean, 41.00 ± 6.83 years) were included in this study. They had a diagnosis of DM1 in the past 9 years to 21 years (mean, 13.64 ± 4.03 years). The mean A1c form of glycohemoglobin (HbA1c) level was 7.38 ± 0.72%. Five patients (45%) were diagnosed with no signs of DR and 6 (55%) with mild NPDR. The eyes with mild NPDR showed one to several spots of hemorrhages and microaneurysms at the posterior pole. The mean duration of diabetes in patients with no DR and mild NPDR was 11.20 ± 1.79 years and 15.67 ± 4.37 years, respectively. All patients had 20/20 best-corrected visual acuity in both eyes and did not complain of any loss of vision or metamorphopsia since the diagnosis of diabetes (Table 1). Eleven healthy subjects (4 males and 7 females; age range, 27–51 years; mean, 38.50 ± 9.10 years) were included as control subjects (Table 2). The average axial length was 23.80 ± 1.14 mm and 23.75 ± 0.92 mm in the DM1 and the control eyes, respectively; the average refractive error was −1.05 ± 1.49 diopters and −0.75 ± 1.64 diopters, respectively. The average RMF_{corr} was 0.280 ± 0.011 mm/°(range, 0.258–0.303 mm/°) and 0.281 ± 0.011 mm/° (range, 0.266–0.303 mm/°) in the DM1 and the control eyes, respectively.

The within-subject standard deviation (σ_w) was <1,400 cones/mm^2 within 460-μm eccentricity. No difference (<1%) was found between the meridians. A summary of the repeatability statistics of cone density measurements along the horizontal meridian is shown in Table 3. Repeatability was 5% to 7% at 230-μm eccentricity, slightly decreasing to 7% to 9% at 350-μm and 460-μm eccentricities, respectively, because of the intrusion of rods that were sometimes misinterpreted as cones by the automated algorithm (Figure 1). A manual check was carried out in each image to minimize the possible error of cone under- or oversampling: the number of cones missed or misinterpreted by the automated algorithm was between 0% and 8.8% across all images.

The PL was well resolved in areas where the SD-OCT, infrared, and color fundus photography did not reveal any pathologic change of the retinal microstructure (Figure 2). The cone density decreased with increasing retinal eccentricity along all meridians ($P < 0.001$) both in DM1 and in control eyes. Statistically significant differences in cone density were measured between DM1 eyes and control eyes at each eccentricity ($P < 0.001$). In the study group, cone density ranged between an average maximum of 50,260 ± 7,842 cones/mm^2 at 230 μm nasal from the fovea to an average minimum of 37,171 ± 6,136 cones/mm^2 at 460 μm superior from the fovea. The average and individual cone density values are shown in Table 4 and Figure 3, respectively. At 230-μm, 350-μm, and 460-μm, the average cone density in the study group was 91%, 90%, and 89% of the average cone density in the control group, respectively. Three cases (Patients 1, 3, and 9), at some retinal locations, showed cone density values above the average estimates of the control group (Table 1 and Figure 3). Age did not significantly interact with the differences in cone density between DM1 and control eyes ($P > 0.05$). The coefficient of variation was 14% and 16% in DM1 eyes and 11% and 10% in control eyes along the horizontal and vertical meridians, respectively. Cone density showed interocular differences of <6% between equivalent eccentricity locations of fellow eyes in all subjects.

The ICD ranged between an average minimum of 4.84 ± 0.34 μm at 230 μm from the fovea and an average maximum of 5.56 ± 0.32 μm at 460 μm from the fovea in the study group. It ranged between 4.61 ± 0.23 μm and 5.24 ± 0.21 μm in the control group, respectively. A summary of the individual and average cone spacing values of both groups is provided as supplementary material (see **Figure**, **Supplemental Digital Content 1**, http://links.lww.com/IAE/A191).

The CRT was 278 ± 20 μm and 260 ± 13 μm ($P < 0.05$) in the study and control groups, respectively. The automated 1-mm central Early Treatment Diabetic Retinopathy Study area thickness was 282 ± 19 μm and 265 ± 9 μm, respectively: the differences between the automated and manual thickness measurements were lower than 6% in all subjects, except for 2 DM1 patients (Patients 8 and 11) and 2 control subjects (D and G). The central PL thickness was 70 ± 3 μm and 71 ± 5 μm ($P > 0.05$) in DM1 and control eyes, respectively; the central ONL thickness was 82 ± 10 μm and 82 ± 8 μm ($P > 0.05$), respectively. Accordingly, the central inner retinal complex thickness was 125 ± 17 μm and

Copyright © by Ophthalmic Communications Society, Inc. Unauthorized reproduction of this article is prohibited.

Table 1. Characteristics of the Study Group (DM1 Patients)

Patient	Age (Years)	Gender	Duration of Diabetes (Years)	HbA1c Level (%)	Diagnosis	Eye	AxL (mm)	BCVA (LogMAR)	CRT (Mean ± SD, μm)	Central PL Thickness (Mean ± SD, μm)	Central ONL Thickness (Mean ± SD, μm)	Central IRC Thickness (Mean ± SD, μm)	10° Retinal Sensitivity (Decibels)
1	36	F	17	6	DR	RE	22.68	0.0	265 ± 16	73 ± 3	72 ± 21	120 ± 15	20.00
						LE	22.46	–0.1	263 ± 20	65 ± 7	86 ± 15	112 ± 14	20.00
2	38	F	21	7.2	DR	RE	23.80	0.0	268 ± 22	68 ± 5	82 ± 19	118 ± 19	20.00
						LE	23.26	–0.1	264 ± 21	63 ± 3	89 ± 17	112 ± 13	20.00
3	36	M	11	8	No DR	RE	24.31	–0.2	287 ± 21	75 ± 2	95 ± 20	117 ± 14	20.00
						LE	24.19	–0.2	286 ± 23	68 ± 8	93 ± 12	125 ± 15	20.00
4	33	M	10	8.2	DR	RE	26.34	0.0	324 ± 20	72 ± 6	92 ± 19	160 ± 15	20.00
						LE	26.44	–0.1	314 ± 26	67 ± 9	86 ± 15	161 ± 17	20.00
5	44	M	11	7.2	No DR	RE	24.20	–0.1	290 ± 17	65 ± 9	102 ± 3	123 ± 10	19.70
						LE	24.06	–0.1	294 ± 24	69 ± 3	94 ± 15	131 ± 15	19.16
6	52	M	16	8	DR	RE	22.88	–0.1	296 ± 28	79 ± 6	86 ± 17	131 ± 17	20.00
						LE	22.90	–0.1	284 ± 25	72 ± 6	68 ± 15	144 ± 15	19.88
7	38	F	19	7.3	DR	RE	25.00	–0.1	295 ± 30	75 ± 5	82 ± 17	138 ± 18	19.88
						LE	24.40	–0.1	294 ± 31	73 ± 5	84 ± 17	137 ± 19	20.00
8	49	M	11	7.8	DR	RE	23.27	–0.1	254 ± 26	67 ± 9	80 ± 11	107 ± 16	19.88
						LE	23.22	–0.1	245 ± 20	69 ± 7	75 ± 14	101 ± 14	19.94
9	39	F	14	8	No DR	RE	22.73	0.0	280 ± 31	75 ± 3	75 ± 20	130 ± 20	19.83
						LE	22.84	0.0	278 ± 30	70 ± 4	72 ± 16	136 ± 19	19.88
10	51	F	11	7.2	No DR	RE	24.77	–0.1	266 ± 20	70 ± 3	84 ± 17	112 ± 13	20.00
						LE	24.46	–0.1	302 ± 22	65 ± 8	81 ± 16	156 ± 16	19.72
11	35	F	9	6.3	No DR	RE	22.69	–0.1	235 ± 20	73 ± 3	61 ± 20	101 ± 15	19.66
						LE	22.79	–0.1	230 ± 10	63 ± 8	61 ± 12	106 ± 10	19.88

AxL, axial length; BCVA, best-corrected visual acuity; F, female; IRC, inner retinal complex; LE, left eye; logMAR, logarithm of the minimum angle of resolution; M, male; RE, right eye; SD, standard deviation.

Copyright © by Ophthalmic Communications Society, Inc. Unauthorized reproduction of this article is prohibited.

Table 2. Characteristics of the Control Group

Subject	Age (Years)	Gender	Eye	AxL (mm)	BCVA (LogMAR)	CRT (M ± SD, μm)	Central PL Thickness (Mean ± SD, μm)	Central ONL Thickness (Mean ± SD, μm)	Central IRC Thickness (Mean ± SD, μm)	10° Retinal Sensitivity (Decibels)
A	34	M	RE	23.69	–0.1	262 ± 20	60 ± 10	86 ± 11	116 ± 22	20.00
			LE	23.62	–0.1	266 ± 18	67 ± 8	72 ± 10	127 ± 21	20.00
B	39	M	RE	22.61	0.0	242 ± 20	73 ± 6	76 ± 6	93 ± 12	20.00
			LE	22.67	0.0	250 ± 21	73 ± 8	74 ± 10	103 ± 15	20.00
C	27	F	RE	23.48	–0.1	258 ± 19	72 ± 8	75 ± 18	111 ± 16	20.00
			LE	23.47	–0.1	259 ± 18	71 ± 9	72 ± 18	116 ± 17	20.00
D	34	F	RE	23.02	0.0	241 ± 15	73 ± 8	82 ± 15	86 ± 13	20.00
			LE	23.12	–0.1	246 ± 19	67 ± 9	88 ± 10	91 ± 13	20.00
E	28	F	RE	23.84	0.0	249 ± 22	74 ± 4	88 ± 11	87 ± 13	20.00
			LE	23.89	0.1	249 ± 20	74 ± 4	89 ± 12	86 ± 14	20.00
F	30	F	RE	24.42	–0.1	262 ± 24	68 ± 3	82 ± 11	112 ± 16	20.00
			LE	24.42	–0.1	251 ± 20	65 ± 7	79 ± 10	107 ± 16	20.00
G	51	F	RE	22.45	0.0	243 ± 24	67 ± 9	73 ± 9	103 ± 16	20.00
			LE	22.23	0.0	241 ± 20	72 ± 8	84 ± 10	85 ± 15	19.94
H	46	M	RE	23.50	0.0	280 ± 19	82 ± 7	81 ± 11	117 ± 13	20.00
			LE	23.41	–0.1	282 ± 16	68 ± 2	86 ± 14	128 ± 12	20.00
I	43	F	RE	23.80	0.0	257 ± 21	74 ± 3	96 ± 15	87 ± 13	20.00
			LE	23.92	0.0	248 ± 17	69 ± 5	103 ± 10	76 ± 11	20.00
L	54	M	RE	25.17	0.0	277 ± 30	73 ± 5	90 ± 12	114 ± 18	19.88
			LE	25.30	0.0	270 ± 28	67 ± 9	85 ± 14	118 ± 19	20.00
M	37	F	RE	25.21	–0.1	286 ± 22	76 ± 8	71 ± 15	139 ± 13	20.00
			LE	25.31	–0.1	292 ± 23	75 ± 8	73 ± 14	144 ± 18	20.00

AxL, axial length; BCVA, best-corrected visual acuity; F, female; IRC, inner retinal complex; LE, left eye; logMAR, logarithm of the minimum angle of resolution; M, male; RE, right eye; SD, standard deviation.

108 ± 18 μm ($P < 0.05$), respectively. The CRT was thinner in women than in men both in the DM1 patients and control subjects. It was 270 μm and 256 μm in women with DM1 and control women, respectively, and 287 μm and 266 μm in men with DM1 and control men, respectively. The interocular differences of CRT were <5% (<15 μm) in all cases, except for a DM1 patient (Patient 10). The interocular differences of the central PL and ONL thicknesses were <10 μm (<14% thickness) in 8 DM1 patients and 9 control subjects.

The multiple linear regression model explained 61% of the variance of cone density (r = 0.61; $P < 0.01$) in the population. Cone density tended to decline with aging (r = –0.33), chronic diabetes (standard r = –0.23), increased HbA1c serum level (r = –0.38), the presence of DR (r = –0.29), and thicker CRT (r = –0.56). Because the HbA1c level statistically highly significantly correlated with the presence of DR (r = 0.85; $P < 0.001$) and the duration of diabetes (r = 0.93; $P < 0.001$), a principal component analysis was used to convert the

Table 3. Repeatability of Cone Density Measurements (50 × 50 μm Sampling Window, Measured Twice) at Various Eccentricities Along the Horizontal Meridian

Group	Eccentricity Location (μm)	Measurement Error (σ_w, Cones/mm^2)	Repeatability (Cones/mm^2)	95% Confidence Interval for Repeatability (Cones/mm^2)	Repeatability (%)
Study group (DM1)	460 temporal	1,201	3,327	2,601–4,053	8.7
	350 temporal	1,149	3,182	2,488–3,877	7.2
	230 temporal	1,030	2,853	2,231–3,476	5.8
	230 nasal	1,261	3,493	2,731–4,255	6.9
	350 nasal	1,118	3,097	2,421–3,773	7.1
	460 nasal	1,096	3,035	2,373–3,698	8.1
Control group	460 temporal	1,335	3,697	2,870–4,524	7.6
	350 temporal	1,298	3,595	2,791–4,399	7.3
	230 temporal	1,325	3,671	2,850–4,492	6.7
	230 nasal	1,078	2,986	2,318–3,653	5.4
	350 nasal	1,279	3,542	2,750–4,334	7.4
	460 nasal	1,363	3,774	2,930–4,618	7.9

Copyright © by Ophthalmic Communications Society, Inc. Unauthorized reproduction of this article is prohibited.

COLOR

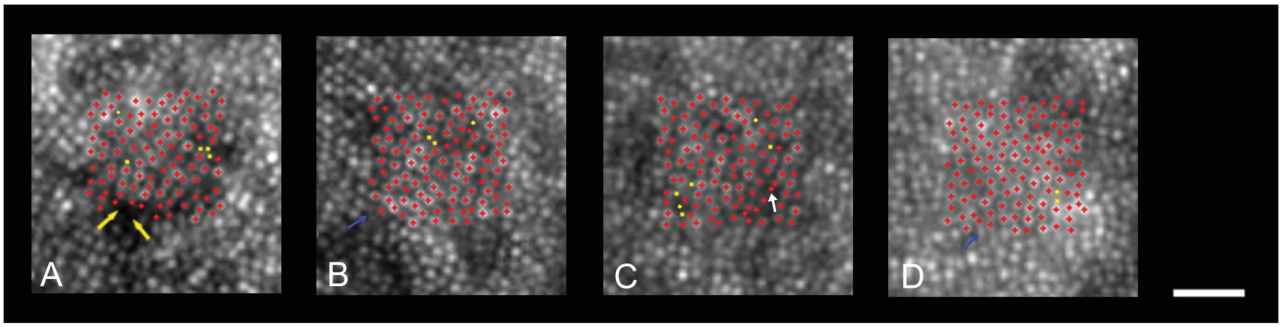

Fig. 1. Performance of the automated cone identification algorithm and potential sources of error in density estimates. Shown are the results of cone labeling performed on a 50 μm × 50 μm sampling windows in 4 representative AO images of 4 different DM1 eyes (**A**–**D**). The sampling window is centered at 460-μm eccentricity (scale bar: 25 μm). Red crosses represent cones identified by the automated algorithm. Yellow squares indicate additional photoreceptors marked by the user: these manually identified cells showed a lower intensity peak and a smaller spacing than cones, probably corresponding to rods, and were not included in cone density estimates by the automated software. At 460-μm eccentricity, the proportion of presumptive rods in each sampling window ranged between 0% and 5%. In general, errors of automated algorithms are because of "point defects" in the image (yellow arrows in **A**), "boundary effects" (i.e., cones at the edge of the sampling window that are not labeled; blue arrows in **B** and **D**), and rods misinterpreted as cones (white arrow in **C**). Manual check of the automated algorithm performance removes cone under- and/or oversampling errors.

correlated variables into a set of values called principal components. The HbA1c level of chronic diabetes and the presence of DR (principal component 1; $P < 0.001$) were therefore found as the variables having the highest influence on cone density decline, followed by aging (principal component 2; $P < 0.001$) and CRT (principal component 3; $P < 0.01$).

Additional images of the retina, located outside the areas of cone density estimation, were acquired to investigate regions of interest in DM1 eyes. In the

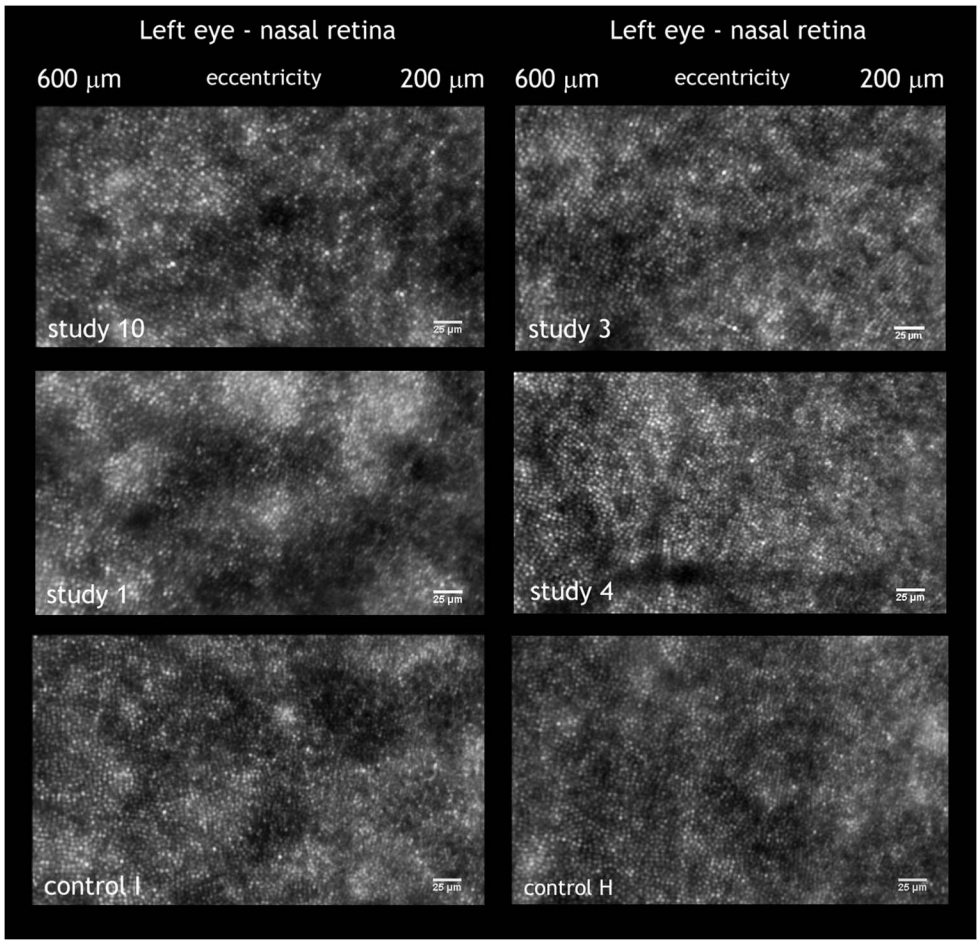

Fig. 2. Adaptive optics retinal images showing the photoreceptor mosaic from 200-μm to 600-μm eccentricity along the nasal retina of the left eye in 6 cases (scale bars represent 25 μm). Upper row: Case 10 and Case 3 are no DR eyes. Middle row: Case 1 and Case 4 are mild DR eyes. Lower row: Case **I** and Case **H** are control eyes.

Copyright © by Ophthalmic Communications Society, Inc. Unauthorized reproduction of this article is prohibited.

Table 4. Cone Density Values Estimated in the Study and Control Group at Various Retinal Eccentricities Along the Horizontal and Vertical Meridians

Retinal Locations	230-μm Eccentricity (Cones/mm^2)	350-μm Eccentricity (Cones/mm^2)	460-μm Eccentricity (Cones/mm^2)
Temporal			
Study group (DM1)	49,577 ± 6,958*	44,086 ± 5,010*	38,093 ± 5,112*
Control group	54,803 ± 6,025	49,033 ± 4,628	42,446 ± 3,439
Nasal			
Study group (DM1)	50,260 ± 7,842*	43,678 ± 6,323*	37,423 ± 5,536*
Control group	54,946 ± 6,974	47,912 ± 4,497	42,680 ± 3,682
Superior			
Study group (DM1)	48,523 ± 7,390*	43,057 ± 6,297*	37,171 ± 6,136*
Control group	53,697 ± 5,433	48,606 ± 4,402	42,413 ± 3,061
Inferior			
Study group (DM1)	47,568 ± 7,522*	43,360 ± 6,321*	37,383 ± 5,956*
Control group	53,360 ± 5,297	48,036 ± 4,507	42,619 ± 4,195

Values are represented as mean ± standard deviation.
*Analysis of variance, $P < 0.001$ (including effect of age).

right eye of a patient (Patient 6) (Table 1; CRT, 296 μm ± 28 μm), there was a focal edema located inferior and nasal from the fovea (this region of interest was located far from the cone counting areas). At the position of the focal retinal edema, the cone photoreceptors were not always resolved (Figure 4). In AO retinal images, the microhemorrhages appeared as dark spots of different shapes and dimensions that could be clearly focused on the inner retina. At the position of the hemorrhage itself, a dark spot with defocused margins was projected onto the PL, completely masking the underlying cell photoreceptors (Figure 5).

The average central 10° retinal sensitivity showed values within normal ranges in all cases, although with a statistically significant difference ($P < 0.05$) between DM1 and control eyes: it was 19.88 ± 0.17 decibels and 19.99 ± 0.03 decibels in DM1 and control eyes, respectively.

Discussion

Several laboratory studies[13,28–30] have shown neural apoptosis, loss of ganglion cell bodies, and glial reactivity in the earliest stages of DR. Experimentally induced diabetes in rats has provided evidence of early cone photoreceptor loss in diabetic retinas[13]: apoptotic cell death, detected via the TUNEL method, was the first pathologic sign evidenced after the onset of diabetes, and it occurred specifically in the outer retinal layers. The retinal neuropathy was also corroborated by previous functional studies in patients with DR,[14,15] where an electrophysiological deficit in both cone and rod system responses at the receptorial level has been shown during diabetes. The decrease in the response has been associated with a loss of photoreceptors and/or a loss of outer segment disk membranes. Deficits both in contrast sensitivity and color vision (loss in sensitivity of the S cone pathway) have been reported

COLOR

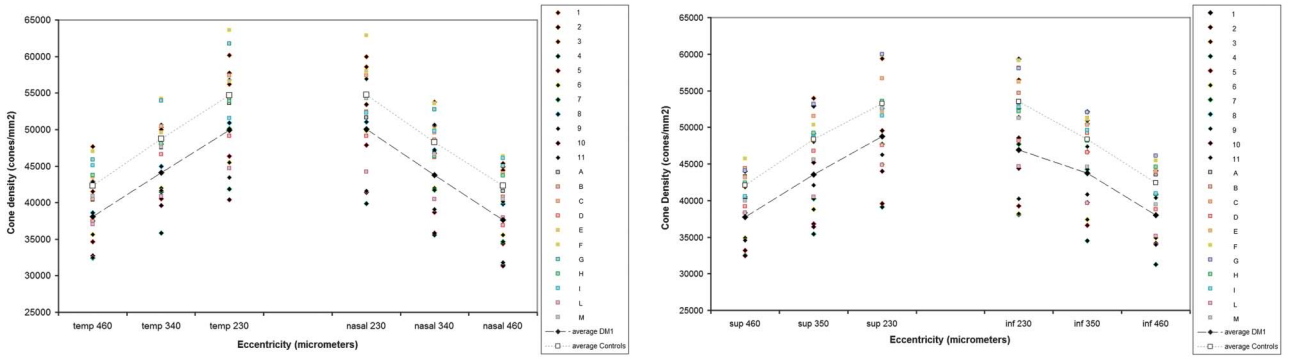

Fig. 3. The average and individual cone density estimates (cones per square millimeter) along the nasal and temporal retina (**A**) and the superior and inferior retina (**B**) in DM1 eyes (black diamonds) and control eyes (gray squares). Cone density was on average 9% to 11% lower in the study than in the control group. The DM1 Cases 1, 3, and 9 showed cone density values above the average of the control group.

Copyright © by Ophthalmic Communications Society, Inc. Unauthorized reproduction of this article is prohibited.

COLOR

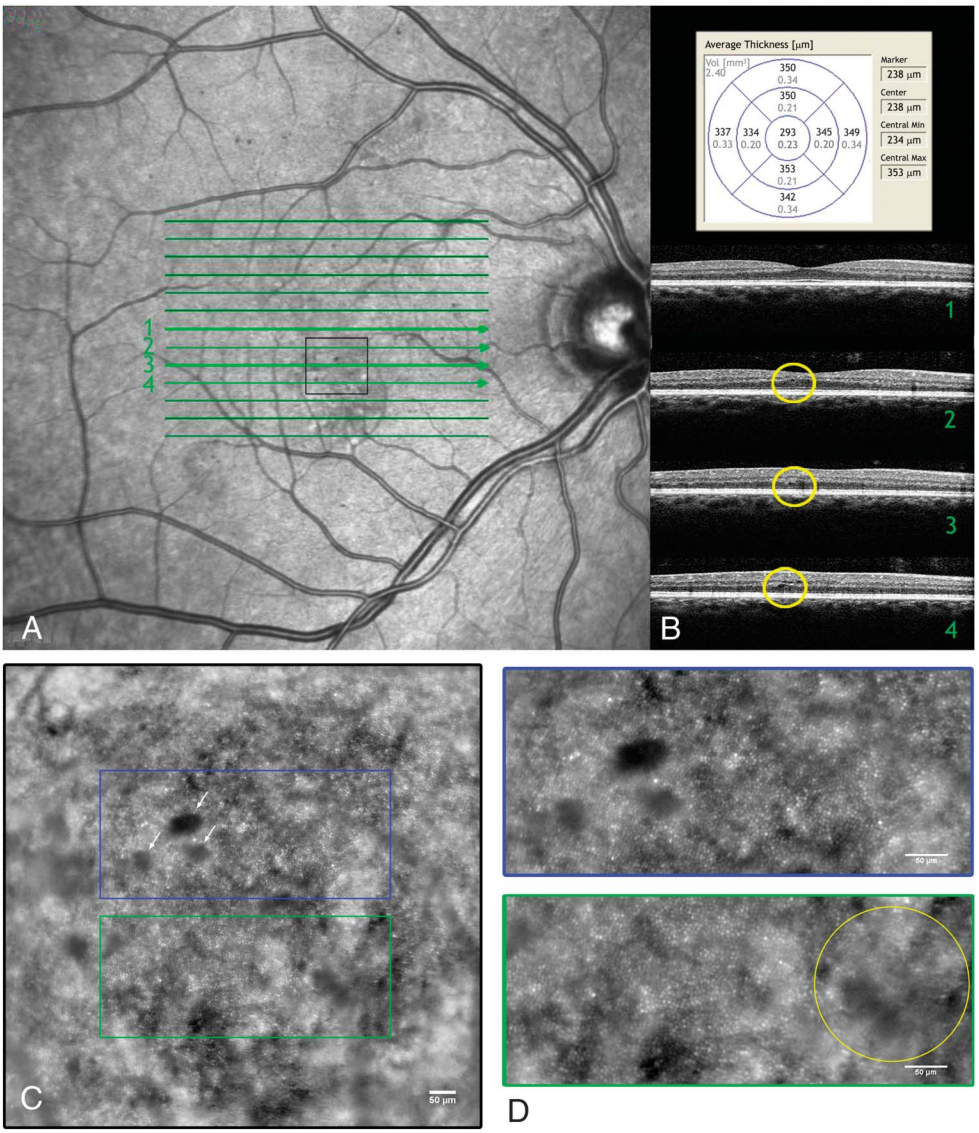

Fig. 4. Effect of intraretinal edema and inner retinal hemorrhages on AO high-resolution imaging of the cone mosaic. **A.** The infrared fundus image of the right eye in a 52-year-old patient with mild DR (Case 6). **B.** The retinal thickness map is shown: the yellow circles in the SD-OCT horizontal scans highlight a focal macular edema. **C.** The edematous retinal area, shown in **A** (black box, 0.96 mm × 1.51 mm), as observed with the AO retinal camera when focusing on the photoreceptor layer. Hemorrhages of various dimensions and shapes (arrows) are spread in the context of the inner retina. The hemorrhages project a dense shadow on the cone mosaic precluding the ability to resolve the underlying cells (masking effect). **D.** Retinal spot hemorrhages (upper inset) completely mask the underlying photoreceptors; nevertheless, the adjacent cones can be well resolved. Conversely, intraretinal edema (lower inset, yellow circle) diffusely scatters light coming from the photoreceptor mosaic and cones and cannot be well resolved. **C** and **D.** Scale bars represent 50 μm.

in background retinopathy.[14,15] Previous studies[14,15,31] have also demonstrated an early involvement of the bipolar and ganglion cells during diabetes. Therefore, it is currently of interest to investigate in vivo the changes occurring to cone photoreceptors during diabetes. High-resolution AO imaging may represent a valid tool to investigate the microstructural retinal changes in diabetic patients.[32] Recently, authors analyzed the microvasculature in a DM1 patient with severe NPDR using an AO scanning laser ophthalmoscopy[33] and in 8 DM1 patients with mild NPDR using a flood-illumination AO retinal camera.[34]

The parafoveal cone density was on average 10% lower in the study group than in the control group at each eccentricity along the horizontal and vertical meridians. The cone density variation was higher in DM1 eyes than in control eyes; most of the variation was found in patients who were diagnosed with diabetes before the age of 30 years. Three DM1 cases (27%) showed cone density values above the average of the control group at some retinal locations: 1 NPDR Case (Case 1) showing an excellent glycometabolic control (HbA1c = 6%) and 2 no DR cases (Cases 3 and 9).

The cone density values of our control group were compared favorably with previous work.[16,18,19,21,25,35–38] In a histologic study, Curcio et al[38] found an average decrease in cone density from approximately 60,000 cells/mm^2 at 0.25 mm to approximately 35,000 cells/mm^2 at 0.5 mm from the fovea in 7 cadaver eyes aged 27 years to 44 years. Li et al[35] found an average cone density of approximately 45,000 cells/mm^2 at 0.30-mm eccentricity from the fovea in 18 subjects aged between 23 years and 43 years using an AO scanning laser ophthalmoscopy. In 2 healthy populations aged between 22

Copyright © by Ophthalmic Communications Society, Inc. Unauthorized reproduction of this article is prohibited.

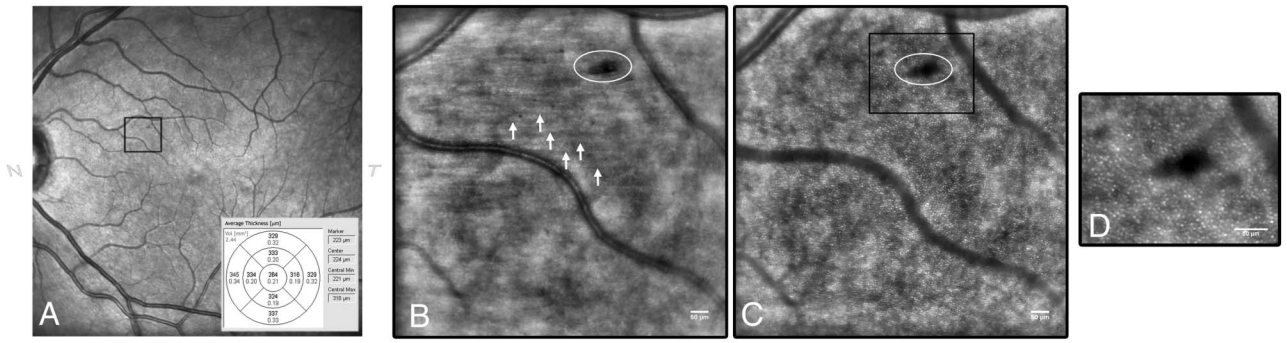

Fig. 5. Adaptive optics imaging of the retinal nerve fiber layer. **A.** Infrared fundus image of the left eye in a 38-year-old female patient with mild DR (Case 2). The retinal thickness map is shown in the lower corner of the scanning laser ophthalmoscopy image. The black box encircles a region of interest (0.92 × 1.45 mm) showing a flame-shaped hemorrhage. **B.** The hemorrhage (encircled; maximum length, 81 μm) could be clearly focused on the retinal nerve fiber layer. The nerve fiber bundles (white arrows) run parallel to each another. **C.** The shadow of the hemorrhage is projected onto the underlying photoreceptor layer showing defocused margins and larger dimension (encircled; maximum length, 98 μm). **D.** High-magnification image of the hemorrhage showing its masking effect on the photoreceptor layer. **B**, **C,** and **D.** Scale bars represent 50 μm.

years to 35 years and 50 years to 65 years, respectively, Song et al[37] found an average cone density of approximately 56,000 cells/mm^2 and approximately 46,000 cells/mm^2 at 0.27 mm, approximately 46,000 cells/mm^2 and approximately 41,000 cells/mm^2 at 0.36 mm, and approximately 38,000 cells/mm^2 and approximately 33,000 cells/mm^2 at 0.45 mm from the fovea, respectively. In the present study, the cone density values of the control group (27–54 years old) was between those of the 2 age-groups measured by Song et al,[37] and it could be reasonably considered as an estimate of the healthy population in this age-group. We also provided estimates of cone density in both eyes of all cases included in the study, finding an average 5 ± 1% interocular difference in cone density, as previously shown.[19,25,38] The interocular differences of CRT were <5% (<15 μm) in all cases, except for 1 DM1 patient.

Although we were unable to estimate the cone density at the fovea, the 10% loss of parafoveal cones in the study group in comparison with the control group was not clinically significant. All patients had 20/20 or better best-corrected visual acuity, and central 10° sensitivity values (±5° corresponding to approximately ±1.4 mm from foveal fixation) were within normal thresholds. Furthermore, in a previous study,[19] we found that at 250-μm eccentricity, an average absolute difference of 7,000 cones/mm^2 between 2 groups of subjects would lead to a difference of <2 cycles/degree of the Nyquist sampling limit of resolution of the cone mosaic.

Approximately 60% of the variance of cone density in the overall population was explained by a multiple regression model containing age, the descriptors of glucose metabolism, and CRT as explanatory variables. Chronic diabetes, the presence of DR, and a higher HbA1c serum level were the variables that mostly influenced the cone density decline in the study population, suggesting that the main part of the cone loss was caused by a prolonged disturbance in the glucose metabolism.

We did not find any statistically significant difference between the central PL or ONL thicknesses of the DM1 and control eyes. The absence of differences between the PL and/or ONL thicknesses of DM1 and control eyes could be related to the relatively small cone density difference (on average 5,000 cones/mm^2) between the study and control groups. This result was consistent with a previous work,[39] where the average ONL + IS (where IS is the inner segment of the photoreceptor) thickness was 88.3 μm and 88.1 μm in 19 eyes with no DR and 20 eyes with DR, respectively, whereas it was 90.9 μm in 40 control eyes (OCT measurements were performed using the OCT-1000; Topcon, Tokyo, Japan). The segmented changes of CRT during diabetes should be further investigated over time. Implementation of AO technology to OCT could bring additional advantages to high-resolution retinal imaging in patients with DR.[40]

In conclusion, AO retinal imaging provided a direct observation of the parafoveal cone mosaic, showing a subtle cone loss in DM1 eyes in comparison with age-matched control eyes. The cone decline was associated with a prolonged disturbance in the glucose metabolism. These preliminary results suggest that changes of the parafoveal cone mosaic may occur in the absence of severe clinical signs of DR or clinically significant macular edema. A prospective analysis of the PL in a large population of patients with no DR and NPDR of increasing severity is needed to understand how the course of the cone mosaic changes during diabetes. Correlation of cone density with functional testing, such as multifocal electroretinogram, and retinal perfusion[41] could advance our understanding between the neural and vascular changes in DR. Furthermore, the development of analysis algorithms for evaluating packing

Copyright © by Ophthalmic Communications Society, Inc. Unauthorized reproduction of this article is prohibited.

arrangement of cones, in addition to cone density, could provide a more sensitive method to describe changes of the cone mosaic longitudinally over time.

Key words: adaptive optics retinal imaging, diabetic retinopathy, cone density, central retinal thickness.

Acknowledgments

The authors are thankful to Marianna Rosati, BSc, and Susanna Lioi, BSc, for archiving the SD-OCT data. The authors also thank Dr. Nicholas Devaney (Applied Optics Group, NUI, Galway) for his comments and revision of the manuscript.

References

1. Resnikoff S, Pascolini D, Etya'ale D, et al. Global data on visual impairment in the year 2002. Bull World Health Organ 2004;82:844–851.
2. Fong DS, Aiello L, Gardner TW, et al. Diabetic retinopathy. Diabetes Care 2003;26:S99–S102.
3. Klein R, Knudtson MD, Lee KE, et al. The Wisconsin Epidemiologic Study of Diabetic Retinopathy XXIII: the twenty-five-year incidence of macular edema in persons with type 1 diabetes. Ophthalmology 2009;116:497–503.
4. Early Treatment Diabetic Retinopathy Study Research Group. Grading diabetic retinopathy from stereoscopic color fundus photographs: an extension of the modified Airlie House classification. ETDRS report number 10. Ophthalmology 1991;98 (suppl 5):786–806.
5. Moore J, Bagley S, Ireland G, et al. Three dimensional analysis of microaneurysms in the human diabetic retina. J Anat 1999; 194:89–110.
6. Kern TS, Engerman RL. Vascular lesions in diabetes are distributed non-uniformly within the retina. Exp Eye Res 1995;60:545–549.
7. Cunha-Vaz JG. Pathophysiology of diabetic retinopathy. Br J Ophthalmol 1978;62:351–355.
8. Barber AJ. A new view of diabetic retinopathy: a neurodegenerative disease of the eye. Prog Neuropsychopharmacol Biol Psychiatry 2003;27:283–290.
9. Verma A, Rani PK, Raman R, et al. Is neuronal dysfunction on early sign of diabetic retinopathy? Microperimetry and spectral domain optical coherence tomography (SD-OCT) study in individuals with diabetes, but no diabetic retinopathy. Eye (Lond) 2009;23:1824–1830.
10. Fletcher EL, Phipps JA, Wilkinson-Berka JL. Dysfunction of retinal neurons and glia during diabetes. Clin Exp Optom 2005;88:132–145.
11. Lieth E, Gardner TW, Barber AJ, Antonetti DA. Retinal neurodegeneration: early pathology in diabetes. Clin Experiment Ophthalmol 2000;28:3–8.
12. Van Dijk HW, Kok PH, Garvin M, et al. Selective loss of inner retinal layer thickness in type 1 diabetic patients with minimal diabetic retinopathy. Invest Ophthalmol Vis Sci 2009;50: 3404–3409.
13. Park SH, Park JW, Park SJ, et al. Apoptotic death of photoreceptors in the streptozotocin-induced diabetic rat retina. Diabetologia 2003;46:1260–1268.
14. Holopigian K, Greenstein VC, Seiple W, et al. Evidence for photoreceptor changes in patients with diabetic retinopathy. Invest Ophthalmol Vis Sci 1997;38:2355–2365.
15. Greenstein V, Sarter B, Hood D, et al. Hue discrimination and S cone pathway sensitivity in early diabetic retinopathy. Invest Ophthalmol Vis Sci 1990;31:1008–1014.
16. Lombardo M, Serrao S, Devaney N, et al. Adaptive optics technology for high-resolution retinal imaging. Sensors (Basel) 2013;13:334–366.
17. Early Treatment Diabetic Retinopathy Study Research Group. Photocoagulation for diabetic macular oedema: early treatment diabetic retinopathy study report number 1. Arch Ophthalmol 1985;103:1796–1806.
18. Lombardo M, Lombardo G, Ducoli P, Serrao S. Adaptive optics photoreceptor imaging. Ophthalmology 2012;119: 1498–1498.e2.
19. Lombardo M, Serrao S, Ducoli P, Lombardo G. Variations in the image optical quality of the eye and the sampling limit of resolution of the cone mosaic with axial length in young adults. J Cataract Refract Surg 2012;38:1147–1155.
20. Li KY, Roorda A. Automated identification of cone photoreceptors in adaptive optics retinal images. J Opt Soc Am A Opt Image Sci Vis 2007;24:1358–1363.
21. Lombardo M, Serrao S, Ducoli P, Lombardo G. Eccentricity dependent changes of density, spacing and packing arrangement of parafoveal cones. Ophthalmic Physiol Opt 2013;33:516–526.
22. Chui TY, Song H, Burns S. Individual variations in human cone photoreceptor packing density: variations with refractive error. Invest Ophthalmol Vis Sci 2008;49:4679–4687.
23. Drasdo N, Fowler CW. Non-linear projection of the retinal image in a wide-angle schematic eye. Br J Ophthalmol 1974; 58:709–714.
24. Coletta NJ, Watson T. Effect of myopia on visual acuity measured with laser interference fringes. Vision Res 2006;46:636–651.
25. Lombardo M, Lombardo G, Lomoriello DS, et al. Interocular symmetry of parafoveal photoreceptor cone density distribution. Retina March 27, 2013 [E-Pub ahead of print].
26. Bland JM, Altman DG. Measurement error proportional to the mean. BMJ 1996;313:106.
27. Bland JM, Altman DG. Measurement error and correlation coefficients. BMJ 1996;313:41.
28. Yu PK, Balaratnasingam C, Morgan WH, et al. The structural relationship between the microvasculature, neurons, and glia in the human retina. Invest Ophthalmol Vis Sci 2010;51:447–458.
29. Yu PK, Balaratnasingam C, Cringle SJ, et al. Microstructure and network organization of the microvasculature in the human macula. Invest Ophthalmol Vis Sci 2010;51:6735–6743.
30. Feit-Leichman RA, Kinouchi R, Takeda M, et al. Vascular damage in a mouse model of diabetic retinopathy: relation to neuronal and glial changes. Invest Ophthalmol Vis Sci 2005;46:4281–4287.
31. Ly A, Yee P, Vessey KA, et al. Early inner retinal astrocyte dysfunction during diabetes and development of hypoxia, retinal stress, and neuronal functional loss. Invest Ophthalmol Vis Sci 2011;52:9316–9326.
32. Carroll J, Kay D, Scoles D, et al. Adaptive optics retinal imaging—clinical opportunities and challenges. Curr Eye Res 2013;38: 709–721.
33. Tam J, Dhamdhere KP, Tiruveedhula P, et al. Subclinical capillary changes in non-proliferative diabetic retinopathy. Optom Vis Sci 2012;89:E692–E703.
34. Lombardo M, Parravano M, Serrao S, et al. Analysis of retinal capillaries in patients with type 1 diabetes and non proliferative diabetic retinopathy using adaptive optics imaging. Retina March 13, 2013 [E-Pub ahead of print].
35. Li KY, Tiruveedhula P, Roorda A. Intersubject variability of foveal cone photoreceptor density in relation to eye length. Invest Ophthalmol Vis Sci 2010;51:6858–6867.

Copyright © by Ophthalmic Communications Society, Inc. Unauthorized reproduction of this article is prohibited.

36. Chui TY, Song H, Burns S. Adaptive-optics imaging of human cone photoreceptor distribution. J Opt Soc Am A Opt Image Sci Vis 2008;25:3021–3029.
37. Song H, Chui TY, Zhong Z, et al. Variation of cone photoreceptor packing density with retinal eccentricity and age. Invest Ophthalmol Vis Sci 2011;52:7376–7384.
38. Curcio CA, Sloan KR, Kalina RE, Hendrickson AE. Human photoreceptor topography. J Comp Neurol 1990;292:497–523.
39. Van Dijk HD, Verbraak FD, Kok PH, et al. Decreased retinal ganglion cell layer thickness in patients with type 1 diabetes. Invest Ophthalmol Vis Sci 2010;51:3660–3665.
40. Miller DT, Kocaoglu OP, Wang Q, Lee S. Adaptive optics and the eye (super resolution OCT). Eye (Lond) 2011;25:321–330.
41. Sakata K, Funatsu H, Harino S, et al. Relationship between macular microcirculation and progression of diabetic macular oedema. Ophthalmology 2006;113:1385–1391.
42. Putnam NM, Hofer HJ, Doble N, et al. The locus of fixation and the foveal cone mosaic. J Vis 2005;5:632–639.
43. Garrioch R, Langlo C, Dubis AM, et al. Repeatability on in vivo cone density and spacing measurements. Optom Vis Sci 2012;89:632–643.
44. Talcott KE, Ratnam K, Sundquist SM, et al. Longitudinal study of cone photoreceptors during retinal degeneration and in response to ciliary neurotrophic factor treatment. Invest Ophthalmol Vis Sci 2011;52:2219–2226.

Appendix

In this study, retinal distances were taken with respect to fixation: while this technique has some errors arising from the inability to accurately determine the distance of the foveal center from the fixation locus, the estimated average distance between the preferred locus of fixation and foveal center was found to be <3 arc minutes (approximately 14 μm) in more than 84% of eyes.[42] By laterally displacing the center of our sampling window by 14 μm, the potential error in our eccentricity-dependent cone density measurements has been estimated to be lower than 1,000 cones/mm^2 at 230-μm eccentricity.[18,19,21,25] The possible error arising from inaccuracy in locating the foveal center was therefore within the measurement error of the cone counting method ($<$1,400 cones/mm^2).

The repeatability of automated cone density estimation was better than 9% within 460-μm eccentricity, with comparable values between DM1 and control eyes. Four previous studies[21,25,43,44] reported statistics for repeated measures of the same retinal location. The estimated error in cone density measurements spanned from approximately 6% to approximately 7.5% within 0.70° eccentricity, favorably comparing to that shown in our study at equivalent eccentricities (i.e., 230 μm). Manual checking of the automated cone counting algorithm performance, as done in this work, is recommended to further minimize the error in density estimates. The error in cone density estimates can be attributed to cone selection, magnification error, distortion in cone images, selection of the region of interest, and sampling area.[21,42] Beyond 400-μm eccentricity, the incorrect identification of rods can be considered as an additional, potential source of error.

Copyright © by Ophthalmic Communications Society, Inc. Unauthorized reproduction of this article is prohibited.